THE ASTROPHYSICAL JOURNAL, 550:1064–1074, 2001 April 1

ANGULAR DISTRIBUTIONS OF SOLAR ENERGETIC PARTICLES

D. V. REAMES, C. K. NG,[1] AND D. BERDICHEVSKY[2]
NASA Goddard Space Flight Center, Greenbelt, MD 20771; reames@milkyway.gsfc.nasa.gov, cheeng@milkyway.gsfc.nasa.gov, xrdbb@lepvx3.gsfc.nasa.gov
Received 2000 September 25; accepted 2000 December 5

ABSTRACT

We report observations, using data from the *Wind* spacecraft, of temporal variations in the angular distributions of H, He, O, and Fe ions at MeV energies during solar energetic particle (SEP) events under a variety of conditions. Detailed time-dependent angular distributions of O and Fe during SEP events are reported for the first time. Extended periods of particle streaming in small gradual events are consistent with continued acceleration that is expected at shock waves driven from the Sun by coronal mass ejections (CMEs). Particles accelerated from SEP events of moderate size show especially strong streaming along the magnetic fields inside an old CME. For the largest events, however, streaming rapidly diminishes, showing behavior that is qualitatively consistent with the theory of Ng et al. In very intense events, that theory predicts rapid growth of proton-generated Alfvén waves, even near and beyond 1 AU, that soon scatter and isotropize the particles. We show, for the first time, cases where SEP streaming is organized by the value of the plasma beta β_p, the ratio of the proton thermal energy to magnetic energy. Higher initial turbulence in the high-β_p plasma may require less additional wave growth to reach significant levels of scattering in the largest SEP events.

Subject headings: acceleration of particles — shock waves — Sun: corona — Sun: particle emission

1. INTRODUCTION

It is now understood that the particles in the large "gradual" solar energetic particle (SEP) events are accelerated at shock waves driven out from the Sun by fast coronal mass ejections (CMEs) and *not* in solar flares (Kahler et al. 1984; Kahler 1992, 1994; Gosling 1993; Reames 1995, 1997, 1999; Lee 1983, 1997, 2000; Tylka et al. 1995; Reames, Barbier, & Ng 1996). The particles that *are* accelerated in impulsive flares have unusually large enhancements in ^{3}He/^{4}He, Fe/O, and $(56 \leq Z \leq 60)$/O of $\sim$1000, $\sim$10, and $\sim$1000, respectively (Reames 1999, 2000), presumably from resonant wave particle interactions in the flare plasma.

In gradual SEP events, the theory of self-generated waves has been used to understand both the acceleration of the particles at interplanetary shock waves in time equilibrium (Lee 1983, 1997; Gordon et al. 1999) and particle transport outward from a source near the Sun (Ng & Reames 1994; Reames & Ng 1998). Recent papers by Ng, Reames, & Tylka (1999a, 1999b) report on a dynamic simulation of the evolution in time and space of the particles and proton-generated waves associated with an outbound shock. As the particles stream out from the shock, different species at the same velocity are scattered differently depending upon their charge-to-mass ratios, Q/A. This model explained the observed (Tylka, Reames, & Ng 1999a, 1999b) systematic variations in element abundance ratios like Fe/O, for example, in terms of differential scattering of Fe and O by the proton-generated Alfvén waves. An additional surprising feature of the model of Ng et al. (1999a, 1999b) was its prediction of the initial behavior of He/H, which can either rise or fall, depending upon the extent of modification of the wave spectrum by high-energy protons (Reames, Ng, & Tylka 2000).

Although the energetic ions sample the wave spectrum over their entire paths from the shock to Earth (and perhaps beyond), it is reasonable to imagine that the abundance variations in gradual events occur primarily near the shock, where the wave intensities are highest. In contrast, particle angular distributions measured near Earth are a more local phenomenon, dependent upon the wave spectrum within about one scattering mean free path of the observer. Another surprise of the theory of Ng et al. (1999a, 1999b) is that sufficiently intense SEP events can significantly reduce the scattering mean free path near Earth when the shock is still at less than 0.5 AU. This should produce observable differences between large and small events whenever the ambient scattering mean free path is large prior to the event. In small events, high anisotropy should persist as long as acceleration continues at the shock. In large events with hard proton energy spectra, the anisotropy will begin to decrease within 6–12 hr of the event onset because of the additional scattering induced by proton-generated Alfvén waves.

Motivated partly by this theoretical interest, we examine the temporal behavior of the angular distributions in a large sample of gradual SEP events with a variety of intensities, spectra, solar longitudes, and conditions in the interplanetary plasma prior to and during the event. SEP and plasma measurements are made on the *Wind* spacecraft, launched 1994 November 1. These are discussed in § 2. We then briefly review relevant features of the theory before examining the detailed behavior observed in SEP events.

2. EXPERIMENTAL METHOD

The angular distributions we discuss in this paper were measured with the Low-Energy Matrix Telescope (LEMT) of the Energetic Particles: Acceleration, Composition and Transport (EPACT) experiment on board the *Wind* spacecraft launched on 1994 November 1 (von Rosenvinge et al. 1995). The spacecraft spins with a 3 s period about an axis normal to the ecliptic. LEMT actually consists of three indi-

[1] Also Department of Astronomy, University of Maryland, College Park, MD 20742.
[2] Also Raytheon-ITSS Corporation, Lanham, MD 20706.

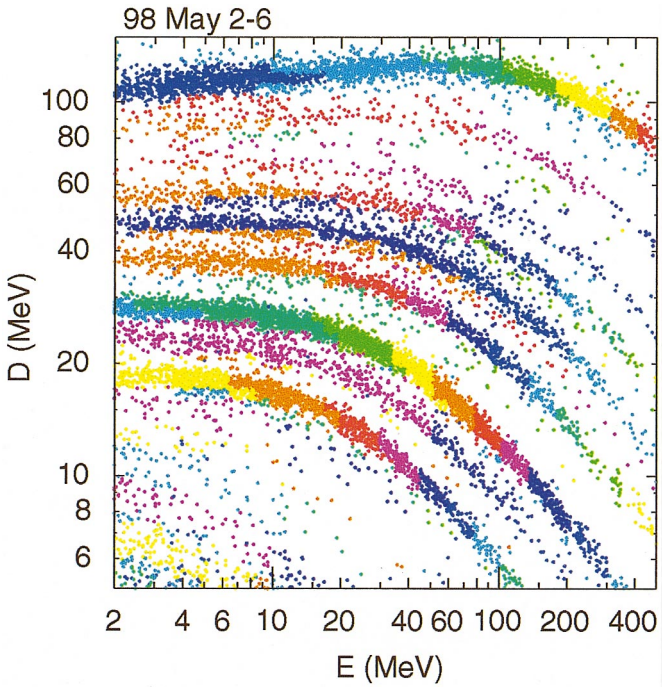

FIG. 1—Onboard bins of particle species and energy identification are indicated with a rotating pattern of colors in a D vs. E pulse-height plot from the LEMT telescope on the *Wind* spacecraft. Onboard identification allows formation of angular distributions for well-identified species and energy intervals.

vidual telescopes; each telescope is a domed array of 16 Si dome (D) detectors, 17 μm thick, followed by a large, 36 cm^2, 1 mm thick detector (E) segmented into 5 × 5 position-sensing strips and backed by an anticoincidence detector. Each telescope views a total opening cone of 126°. The axis of the central telescope lies in the ecliptic plane, orthogonal to the spin axis, while the other two telescopes are inclined 25° above and below the ecliptic plane to provide all-sky coverage as the spacecraft spins (see von Rosenvinge et al. 1995). The total geometry factor of LEMT is 51 cm^2 sr.

A section of a D versus E pulse-height plot from LEMT is shown in Figure 1 for a region that covers elements from C through Fe; different species and energy bins identified by an onboard algorithm, described in the Appendix, are shown with an alternating pattern of colors. Angular distributions for individual species and energy intervals can be formed on board relative to the direction of the Sun or the magnetic field as described in detail in the Appendix. Only magnetic-sectored data are presented in this paper.

3. SCATTERING AND WAVE GROWTH

The theory of Ng et al. (1999a, 1999b) follows the evolution of the distribution function of particles in momentum p, pitch angle μ, time t, and position r, along a magnetic flux tube. The effects of pitch-angle diffusion, convection by the solar wind, and adiabatic deceleration are included (Ng et al. 1999b). Wave intensities are followed in wavenumber k, time, and space. Equations governing the particles and waves are coupled through the particle diffusion coefficient, which depends upon the wave spectrum and the wave growth rate, which depends upon the gradient of the proton distribution function in μ and p. Ions are injected at the position of the shock with power-law spectra and coronal abundances. Initially, a background Kolmogorov wave spectrum with a $k^{-5/3}$ dependence is assumed.

Figure 2 shows a typical example of the time evolution in the spectrum of outward-streaming Alfvén waves near 1 AU in a large event similar to that of 1998 April 20 (Ng et al. 1999a). The initial ambient wave spectrum produces a scattering mean free path, $\lambda \sim 1$ AU, as is typically deduced from the profiles of small impulsive flare events that serve as test particles that do not modify the interplanetary medium (e.g., Mason et al. 1989; Tan & Mason 1993).

Also apparent in Figure 2 is a historic discrepancy (see, e.g., Fisk 1979, and discussion in Reames 1999) between wave spectra consistent with particle-scattering measurements and typical power spectra observed by a magnetometer (e.g., Leamon et al. 1998), shown as a heavy dashed line in Figure 2. If one envisions interplanetary magnetic flux tubes as loosely tangled spaghetti being convected past a spacecraft (Jokipii & Parker 1969; Fisk & Jokipii 1999; Giacalone & Jokipii 1999; Giacalone, Jokipii, & Mazur 2000), a magnetometer on that spacecraft will see an intense spectrum of field variations passing from strand to strand, while energetic particles in the medium see much smaller variations as they propagate along a single strand. As can be seen from Figure 2, the proton-generated waves only begin to compare with the ambient magnetic turbulence late in the event, as the shock approaches Earth. Thus, proton-generated Alfvén waves have been observed directly only near shocks (e.g., Kennel et al. 1986; Tan et al. 1989; Gordon et al. 1999; Berdichevsky et al. 1999).

Thus, while magnetic power spectra are not quantitatively related to Alfvén wave spectra, the general state of plasma turbulence is surely relevant for particle scattering, if only because of the higher probability of magnetic mirror conditions in turbulent plasma. It has been known for many years (Burlaga, Ogilvie, & Fairfield 1969) that microscale

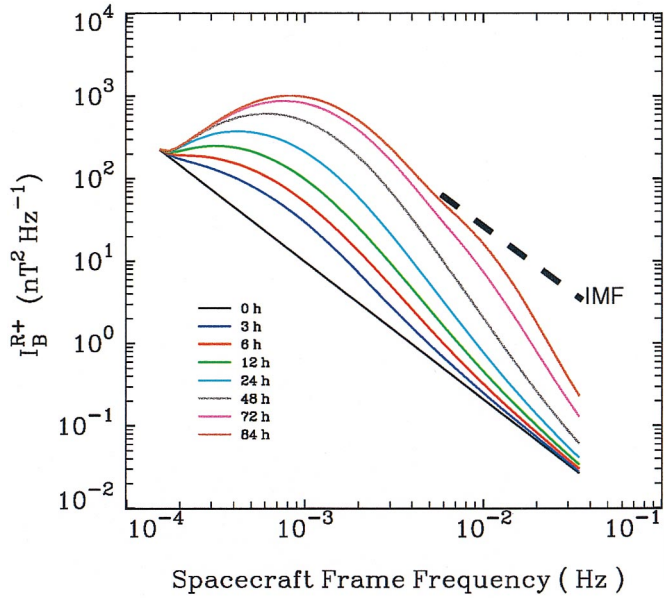

FIG. 2—Time evolution in the spectrum of right-hand outbound Alfvén waves at 1 AU calculated for a large SEP event by Ng et al. (1999a). Spectra remain below the typical interplanetary turbulence spectrum (IMF) seen by a magnetometer (e.g., Leamon et al. 1998) until late in the event near the time of shock passage. Magnetometers respond to convected spatial structures that SEP particles do not see. The initial wave spectrum corresponds to $\lambda \sim 1$ AU.

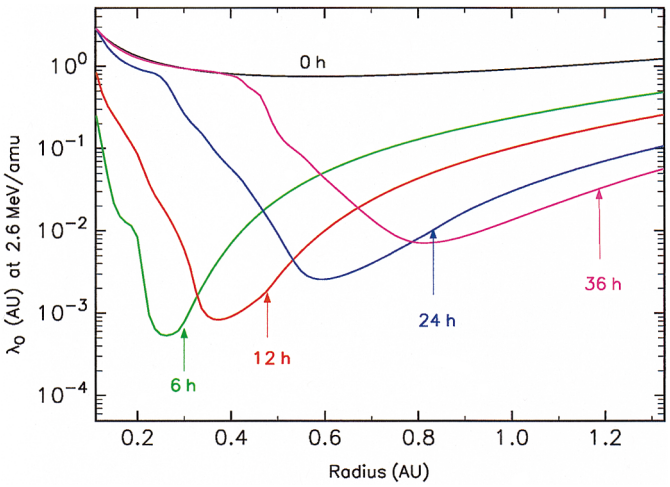

FIG. 3—Evolution of the scattering mean free path λ of O in space and time according to the model of Ng et al. (1999b). While the greatest decrease in λ occurs near the shock, its value at 1 AU also decreases substantially after a few hours. Initially, $\lambda \sim 1$ AU.

fluctuations in the plasma are strongly correlated with the plasma beta β_p, the ratio of proton thermal energy E_p to magnetic energy E_M. Burlaga et al. (1969) found that when $E_p > E_M/2$, conditions were very disturbed with fluctuations on a timescale of $\sim$1 minute to $\sim$1 hr. For a typical solar-wind speed, these timescales map to spatial scales comparable with the gyroradii of ions in the 2–10 MeV amu^{-1} region that we study. In our study, therefore, we use β_p, or specifically, $\beta_p > 0.5$ as a proxy for high plasma turbulence.

Figure 3 shows the evolution of λ as a function of space and time from the simulation of Ng et al. (1999b). The minimum value of λ as a function of r follows the shock outward. Small values of λ are required for acceleration at shocks (Lee 1983). However, the feature of relevance here is the decrease in λ as a function of time near 1 AU. This behavior will affect angular distributions in SEP events that are as large as the one simulated in Figure 3. Many aspects of this theory are preliminary and require further study. However, its qualitative success in understanding and predicting a wide variety of complex abundance variations suggests that we seriously examine its predictions for angular distributions at 1 AU.

4. SMALL EVENTS

The growth rate for Alfvén waves depends upon the intensity of protons as well as their angular distribution (Stix 1962; Melrose 1980). Therefore, we first examine events with low proton intensity, below the streaming limit (Reames 1990; Ng & Reames 1994; Reames & Ng 1998), that are least likely to perturb the local plasma, even when their streaming is highly anisotropic.

Figure 4 shows the time evolution of intensities and angular distributions for various particle species during an event on 2000 May 1 associated with an impulsive flare at W61°. The 16 sectored angular distributions measured relative to the magnetic field show a strong field-aligned flow initially that declines rapidly, as do the particle intensities. Particles of velocity, v, from an impulsive injection at the Sun begin to isotropize on a timescale of $2\lambda/v$ that is $\sim$6 hr in this event, corresponding to $\lambda \sim 1.5$ AU. He ions of 5–8 MeV amu^{-1} arrive earlier than those of 2.5–5 MeV amu^{-1}, and they also isotropize earlier. Lower intensities of O and Fe make measurements more difficult, but these ions seem to follow the same pattern as He of the same velocity. The event of 2000 May 1 has the "typical" behavior of a small impulsive event (e.g., Mason et al. 1989), except that intensities are sufficiently high to allow us to measure angular distributions for the rarer species.

In contrast with the event of 2000 May 1, Figure 5 shows the small gradual event 1998 June 16 from a CME-associated event at W90°. In this event, modest intensities persist for over 2 days, and particle streaming can be seen for more than a day. Here the particle angular distributions peak near 180°, rather than 0°, only because the field polarity has changed. The field polarity reverses at about 0800 UT on June 18, but the flow has become more isotropic before that time. The continuous particle flow is consistent with continued acceleration at the CME-driven shock.

In Figure 6, we quantify the magnitude of the streaming in the 1998 June 16 event, and in a similar, somewhat larger event on 1999 January 20. Here we define a front/back ratio, F/B, by summing the intensities hourly in the two magnetic sectors spanning the forward direction and dividing by intensities in the two sectors spanning the backward direction. F/B is defined to be ≥ 1, and because of quantization of the readout, the ratio varies between 1 and $\sim$100. Accuracy near 1 does not exceed $\sim$1%. The solar-wind speed and proton density are also shown on the plots, as are the magnetic field strength and direction. The plasma beta, β_p, the ratio of proton thermal energy to magnetic energy is also shown in the figure; regions with $\beta_p < 0.5$ are shaded in red. Times of event onset and shock passage are noted in the figure.

For both events shown in Figure 6, F/B begins at a value of $\sim$4 for protons and remains above 2 for 18–24 hr. The value of F/B scales roughly as $1/v$ for the two He energy intervals as expected from diffusion theory. For protons, F/B may be higher partly because of the lower velocity interval. At the onset of the 1998 June 16 event, intensities only rise above background by a factor of $\sim$10. This background limits the maximum attainable value of F/B. Large variations in F/B occur on different flux tubes being convected past the spacecraft. These variations are common but are not well understood in detail. Regions of low β_p have little apparent effect on F/B in the 1998 June event but span most of the region of highest F/B in the 1999 January event. A well-defined shock is noted on 1999 January 22, and some level of anisotropy persists until shock passage. The increase in the solar-wind speed, density, and the magnetic field intensity at about 2000 UT on 1998 June 18 may be the remnants of a former shock.

5. EVENTS WITHIN CME EJECTA

In some cases, a new CME and shock may be launched at the Sun to provide a new onset of SEP acceleration while an observer is completely immersed in an older interplanetary CME that extends past 1 AU. The relatively small events in 1998 May 2 and 6, shown in Figures 7 and 8, occur during the passage of well-defined ejecta. The rotation in the magnetic-field azimuth angle of a well-known magnetic cloud can be seen on May 2–3 in Figure 8. The region of high density on May 3 is a cold plasma cloud with high abundances of He^+ (Gloeckler et al. 1999). The CMEs

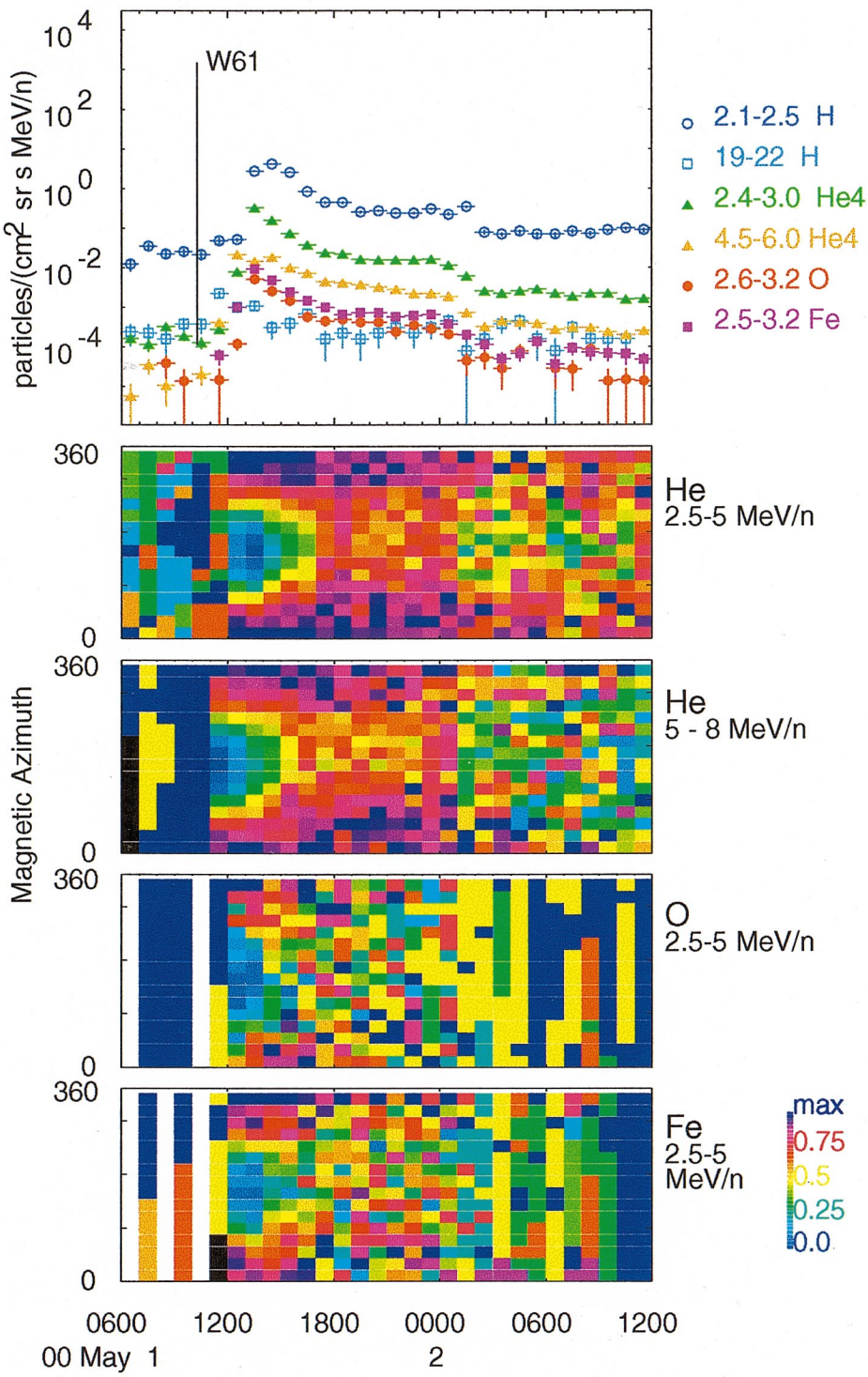

FIG. 4—Angular distributions of He, O, and Fe ions, relative to the magnetic field direction are shown for the indicated energy intervals for the impulsive-flare associated event of 2000 May 1. Colors indicate intensity scaled to 1 at the maximum intensity for each hour. Intensity-time profiles for various species are shown in the upper panel.

driving the acceleration in the events of both May 2 (W15°) and May 6 (W65°) have speeds in excess of 1000 km s^{-1}; a smaller event late on May 3 (W34°) has a CME speed of only 705 km s^{-1} and no obviously associated SEP event.

The F/B ratios early in the events of May 2 and May 6 are extremely large. In the event on May 2, the ratio may be limited initially by the presence of preevent background. F/B for protons drops suddenly from ~20 to ~3 as the spacecraft enters the cold, dense cloud late on May 2, then drops suddenly again about 18 hr after onset. In the event on May 6, F/B falls from an initial value of ~100 to a value of ~4 while β_p rises from ~0.01 to 0.1. That value of ~4 then persists until about 22 hr after event onset. The value of β_p is very low during most of the May 2–8 period. Periods of declining F/B do occur during rising β_p. In addition, F/B falls suddenly on May 7 just as β_p suddenly rises to ~1.

Another small event that is launched inside a magnetic

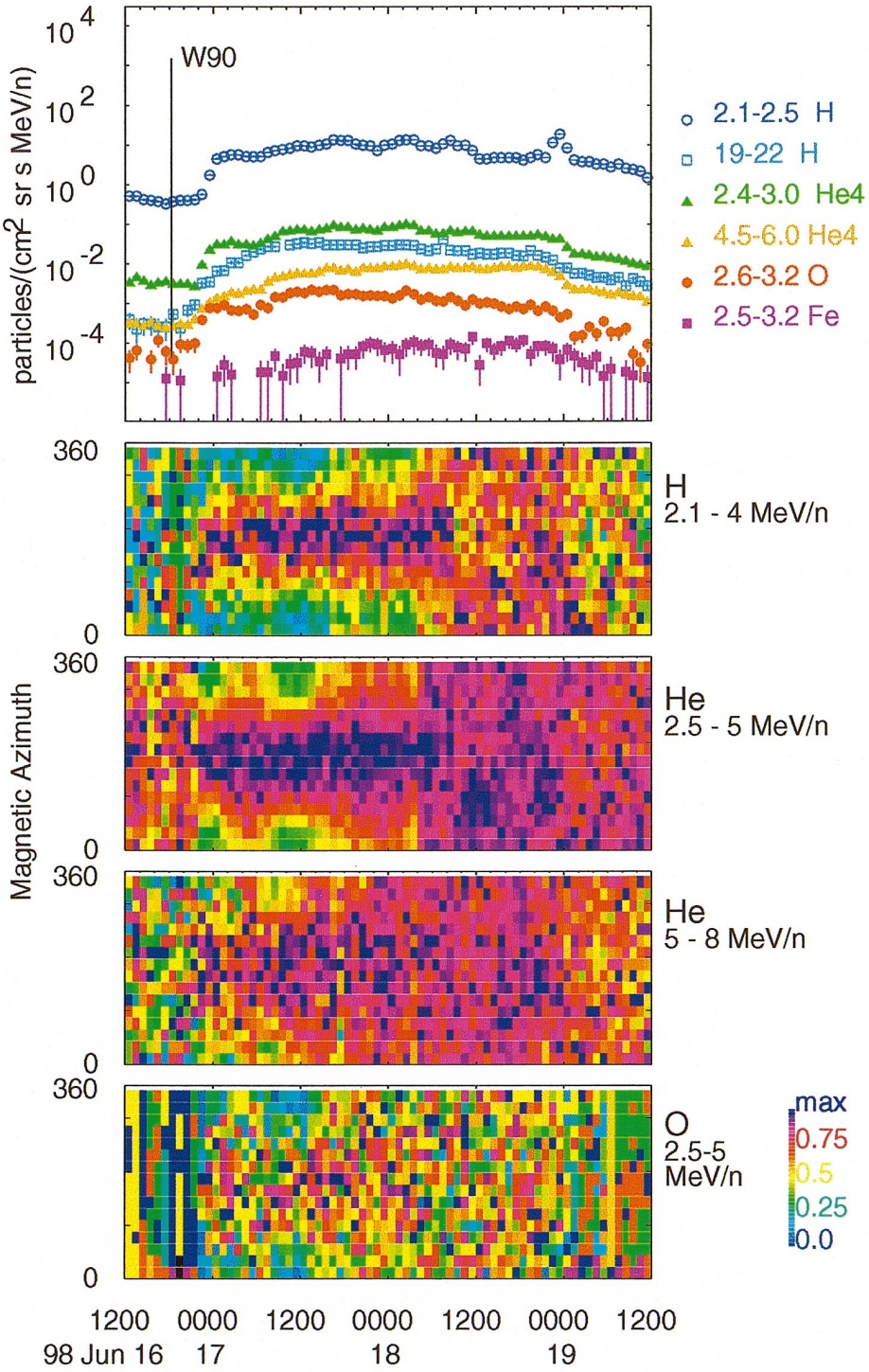

FIG. 5—Angular distributions of H, He, and O ions, relative to the magnetic field direction are shown for the indicated energy intervals for a small gradual event associated with a 1200 km s^{-1} CME on 1998 June 16. Note that the field polarity has reversed from that in Fig. 4. Colors indicate intensity scaled to 1 at the maximum intensity for each hour. Intensity-time profiles for various species are shown in the upper panel.

cloud and has an initial value of F/B $\sim$ 100 for several hours is the W33° event of 1997 November 4 (not shown). Together these events show the importance of the detailed interplanetary environment in supporting and controlling particle streaming. They also show evidence of persistent acceleration at the CME-driven shock. However, it is difficult to determine whether decreases in streaming result (1) from a decrease in acceleration with time, or (2) because the spacecraft has moved into plasma with greater scattering or (3) with a magnetic connection to a weaker region of the source. Nevertheless, proton-generated waves are unlikely to be a factor far from the source in these events.

6. LARGE SEP EVENTS

When SEP proton intensities remain at the streaming limit (Reames & Ng 1998) for extended periods of time, proton-generated waves may soon begin to influence the local transport. Since 2.5 MeV amu^{-1} ^{4}He resonates with

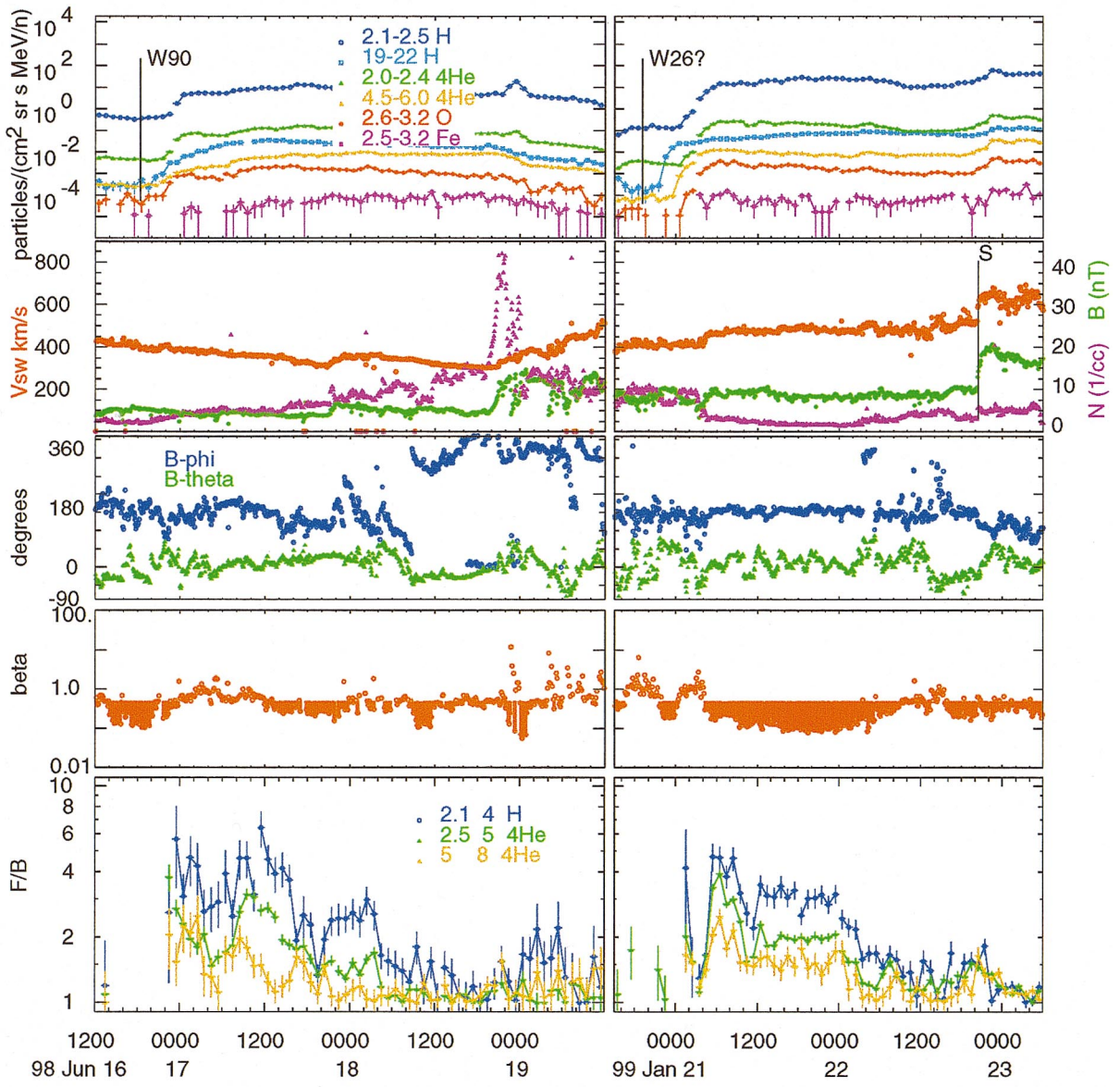

FIG. 6—Particle intensities and plasma parameters are shown for the small gradual events of 1998 June 16 and 1999 January 20. Front/back ratios, F/B, are shown in the lower panels for H and He. Plasma beta β_p is plotted in the next panel with regions with $\beta_p < 0.5$ shaded red.

waves produced by ~10 MeV protons, spectra must be relatively hard to affect the scattering of He and especially heavier ions with $Q/A < 0.5$.

Figure 9 shows SEP and plasma parameters for the large events of 1998 September 30 at W78° and 2000 April 4 at W66°. Protons of 2.1–2.5 MeV rise above 1000 (cm^2 sr s MeV)$^{-1}$ in both events and remain high for days. However, spectra are much harder in the September 30 event, as seen by the much higher intensity of 19–22 MeV protons in the figure. Hard proton spectra in the 1998 September 30 event were shown to produce rising He/H ratios by preferentially scattering He early in the event (Reames et al. 2000); soft spectra in the 2000 April 4 event are unable to affect He/H.

For the 1998 September 30 event shown in Figure 9, F/B begins at a value of ~2, rapidly declines, and remains low, while β_p remains high during most of the event. For the event of 2000 April 4, F/B begins at a value of ~3, and declines slowly and irregularly below 1.5 over a period of ~12 hr. A period of low β_p lasts throughout the event except for the first few hours. During the initial few hours of the April 4 event, 2.1–4 MeV H is scattered more than 2.5–5 MeV amu^{-1} He and O, a *very* unusual situation. Waves that resonate with 2–4 MeV H may be self-generated by the high intensities of H; however, the 2.5–5 MeV amu^{-1} He and O resonates with waves that would be generated by greater than 10 MeV H that is scarce because of the steep H spectrum.

Finally, Figure 10 compares the large events of 1998 April and August at solar longitudes of W90° and E9°, respectively. Both events begin with moderately high F/B ~ 8 during periods of low β_p. F/B has declined to values of less than 2 in 6–8 hr in both events. This rapid decline in these large events is to be compared with the persistently high F/B for the small events in Figure 6.

However, F/B is also strongly controlled by β_p for the events in Figure 10. For the 1998 April 20 event, F/B

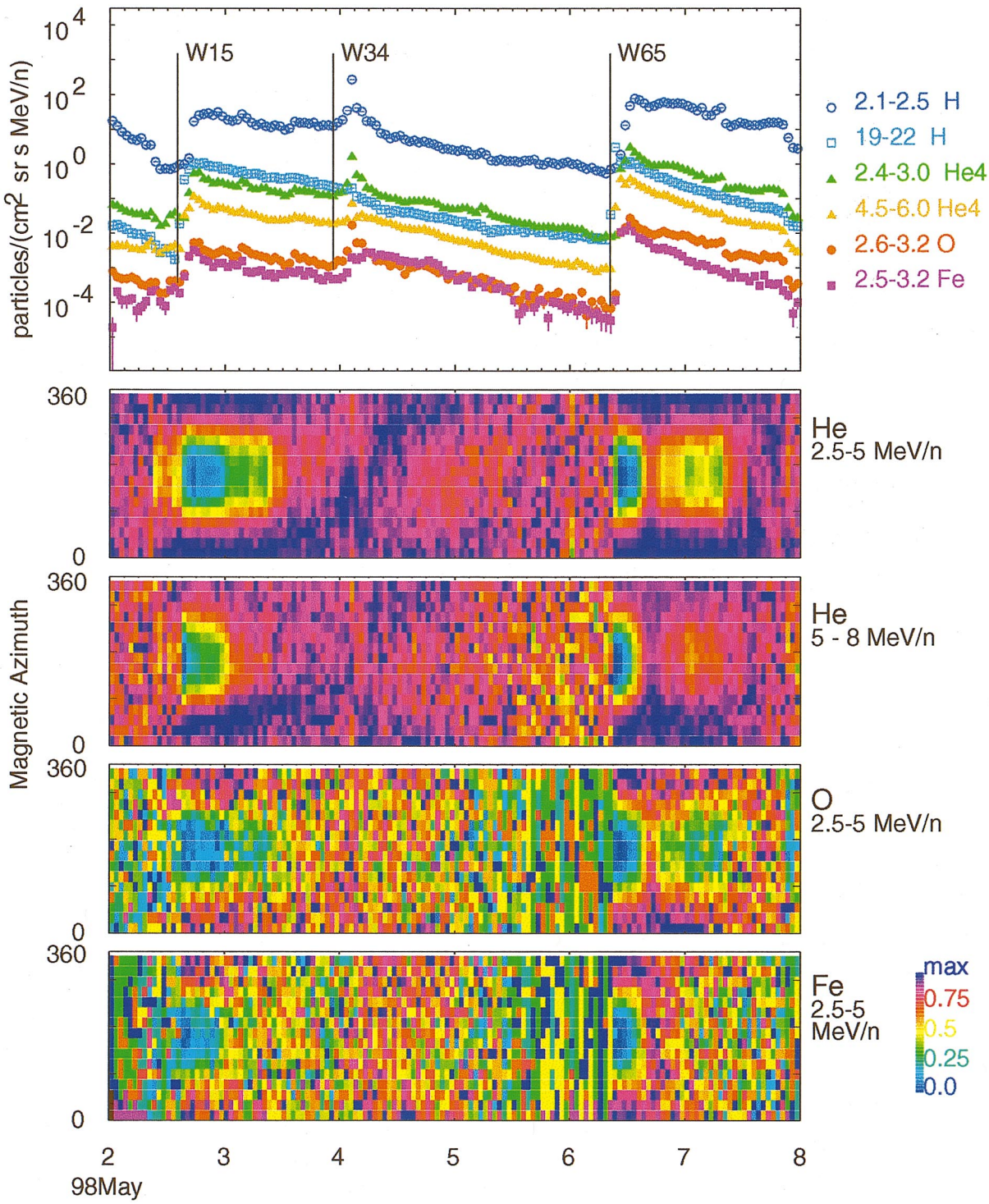

FIG. 7—Angular distributions of H, He, O, and Fe ions, relative to the magnetic field direction are shown for the indicated energy intervals for the period 1998 May 2–8, as in Figs. 2 and 5. Deep and persistent anisotropies are seen in the SEP events of May 2 and May 6 associated with CMEs with speeds greater than 1000 km s^{-1}. A 705 km s^{-1} CME late on May 3 shows no additional SEP contribution. The May 2 and 6 events occur during ejecta from earlier CMEs from the same active region.

returns to 1 early on April 21 just as β_p rises above 0.5. Two subsequent peaks in F/B on April 21 correspond to excursions of β_p below 0.5. After more than a day with F/B $\sim$ 1 and high β_p, F/B suddenly rises again at $\sim$1400 UT on April 23 when β_p again falls to low values. This unusual resurgence of streaming begins 2 days after event onset and occurs during a period of *declining* particle intensities. This resurgence in F/B does not correspond to a new injection of energetic ions; rather, it occurs when the spacecraft moves into a region of low-beta plasma where ions have actually diminished in intensity after 2 days of continued streaming from the shock.

While particles from the 1998 August event generally propagate through low-beta plasma, as shown in Figure 10,

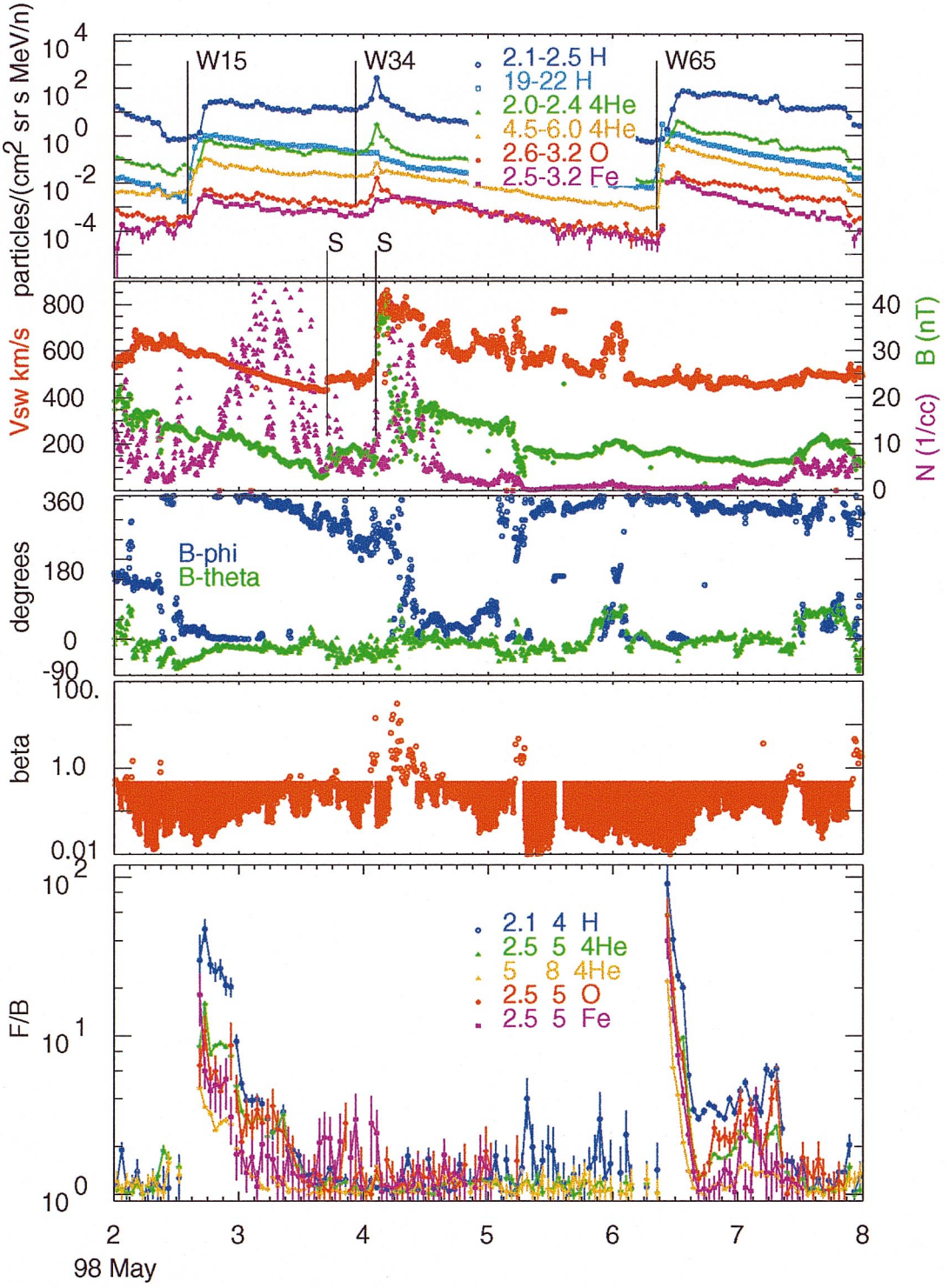

FIG. 8—Particle intensities and F/B ratios are shown for H, He, O, and Fe, along with plasma parameters (as in Fig. 6) for the 1998 May 2–8 period. Extremely strong particle streaming is seen during periods of unusually low beta early in the events of May 2 and 6.

valleys in F/B do correspond to upward excursions in β_p to values greater than 0.5.

7. SUMMARY AND CONCLUSIONS

We have explored the evolution in the angular distributions of energetic ions in SEP events under a wide variety of circumstances. In general, ion streaming depends upon the duration of acceleration, ion intensities, and conditions of the background plasma.

1. For small events with intensities too low to modify the plasma, the duration of the streaming is most strongly affected by the duration of the source. Streaming lasts for only a few hours for flare-associated particles but can persist for more than a day in gradual, shock-associated events. In these latter events, ions continue to stream through plasmas of high and low beta, although greater streaming occurs in low-beta plasma.

2. Ions that stream through the magnetically dominated

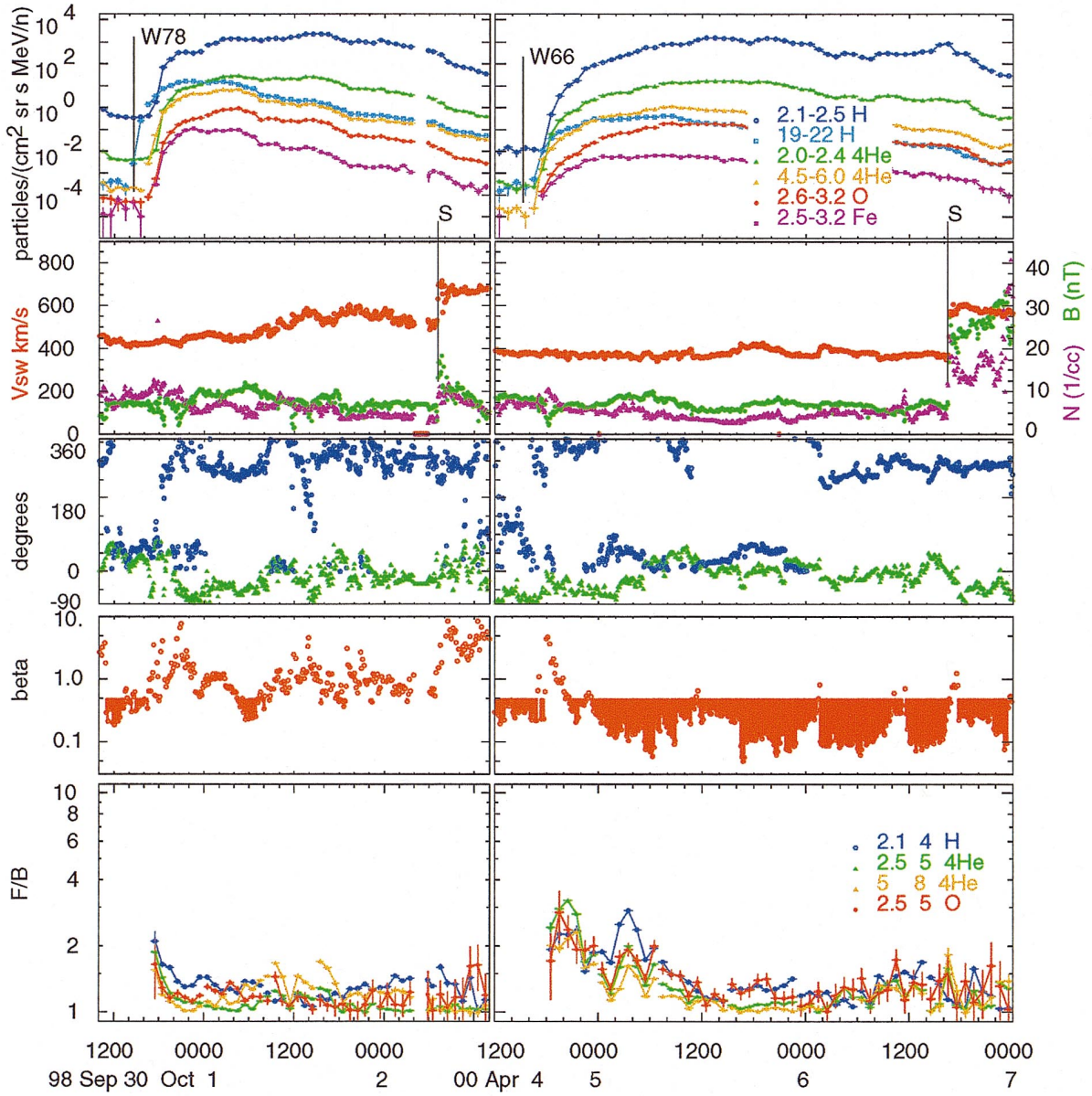

FIG. 9—Particle intensities and F/B ratios are shown for H, He, and O, along with plasma parameters, for the large SEP events of 1998 September 30 and 2000 April 4. Note expansion of scales for beta and F/B compared with Fig. 8. Streaming remains low throughout the high-beta 1998 September event and is relatively low, despite low beta, in the 2000 April event.

plasma inside a magnetic cloud or ejecta of a CME can be *highly* anisotropic. Streaming with $F/B \geq 4$ can persist for 18–24 hr. In this time interval ~ 2 MeV amu^{-1} ions can traverse ~ 12 AU. One can easily imagine reflection from distant magnetic compression regions as a dominant mechanism for filling the backward cone; however, the angular distributions show no direct evidence of bidirectionality or of a single reflection.

3. Particle streaming is often, but not always, organized by the plasma beta. Streaming of ions is more sensitive to beta in large SEP events than in small ones.

4. In large SEP events, we find no case where streaming with values of $F/B > 2$ lasts more than ~ 6 hr.

Small gradual events show us that particles continue to stream freely away from the shock for long periods of time; streaming may diminish in high-beta plasma, but it is not completely suppressed. The rapid decrease of streaming in large SEP events is qualitatively consistent with models that predict local Alfvén-wave growth (Ng et al. 1999a, 1999b). This wave growth may be more effective in high-beta regions, where turbulence is already large, than in low-beta regions, where the ambient wave spectra may be much lower.

We thank K. Ogilvie for the use of plasma data from the Solar Wind Experiment (SWE) and R. Lepping for use of data from the Magnetic Field Experiment (MFE), both on the *Wind* spacecraft. We also thank A. Tylka for many helpful discussions during the course of this work.

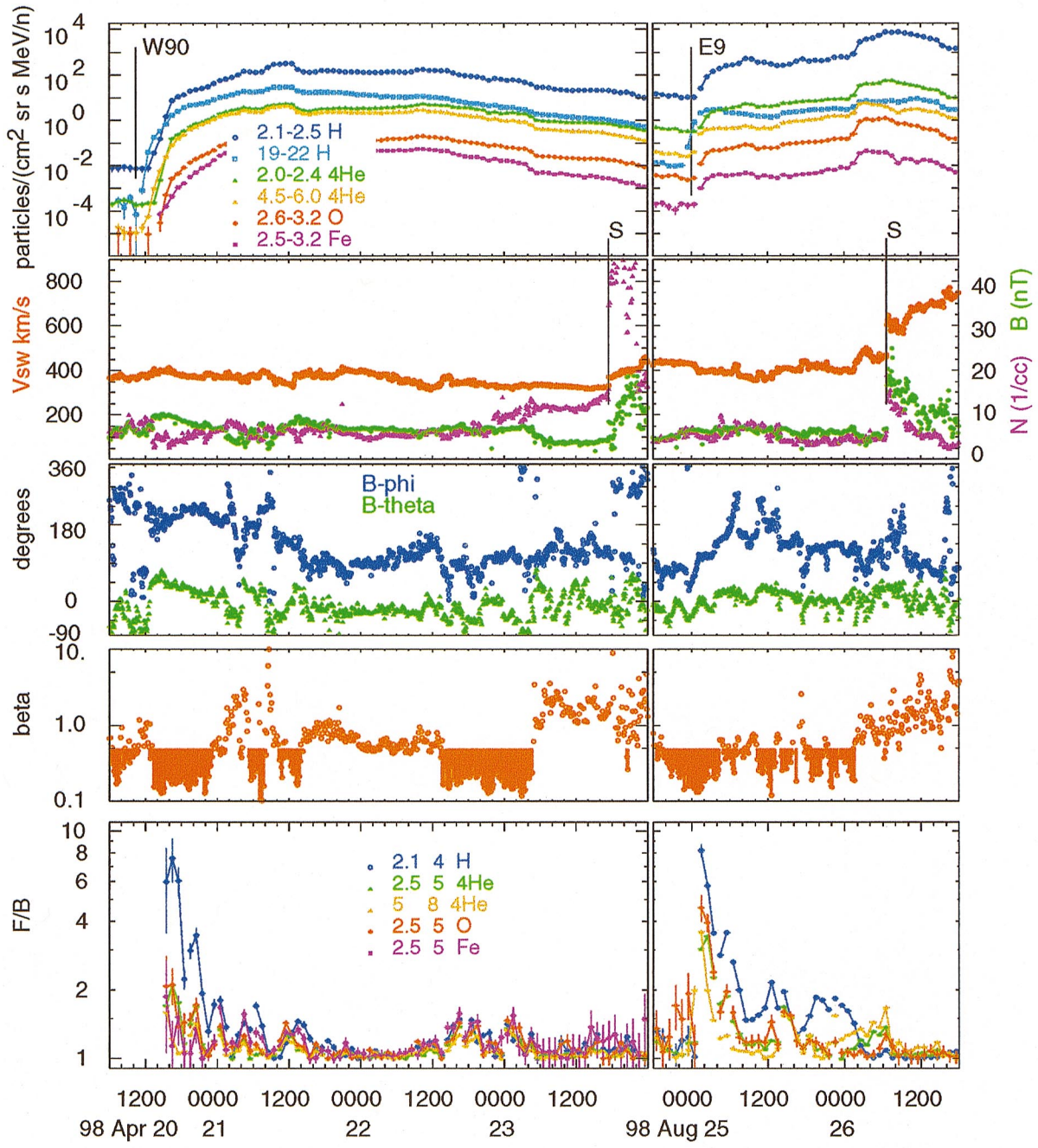

FIG. 10—Particle intensities and F/B ratios are shown for H, He, O, and Fe, along with plasma parameters, contrasting large SEP events of 1998 April 20 from W90° and 1998 August 24 from E09°. Streaming decreases rapidly initially in both events but then diminishes during high-beta periods and recovers again in low-beta periods.

APPENDIX

ONBOARD EVENT PROCESSING IN THE LEMT TELESCOPES

Because of the high particle rates implied by the LEMT's large geometry, each of the three telescopes is served by a UTMC UT1750 event processor that can process pulse heights in the D and E detectors and directional information at a the rate of 12,000 particles s^{-1}. As a part of this processing, particle arrival directions in a telescope are determined by lookup in a 400 element (16 D detectors $\times$ 5 $\times$ 5 positions in E) table that provides the mean elevation, azimuth, and path length through the D detector. The incoming 16 bit D and E pulse heights are converted to logarithms, corrected for path length in D, and combined to enter one of two 4 Kbyte lookup tables (one for H and He, the other for $Z \geq 6$) to determine particle species and energy. Resultant particles are accumulated in one of 150 species and energy bins. Onboard species identification and binning may be confirmed using sample pulse heights and their assigned bins that are telemetered at a rate of $\sim$1 particle s^{-1}. A section of pulse-height matrix is shown in Figure 1 for a region that covers elements from C through Fe; different species and

energy bins identified on board are shown with an alternating pattern of colors. With onboard identification, LEMT can process 36,000 times as many particles as telemetry alone would allow. This rate has been adequate to permit processing of *all* pulse heights acquired on board. However, this is partially because protons are sampled only by the front-end electronics.

For selected particle species and energy intervals, angular distributions may be derived by combining the arrival direction in the telescope with the spin phase relative to the direction of the Sun or the magnetic field and binning them accordingly. The magnetic azimuth is provided on board *Wind* from the Magnetic Field Experiment (MFE) during each 3 s spin. In general, LEMT can provide directional data for a specific species and energy bin in one of three formats: (1) Sun-sectored in 8 azimuthal bins, projected in the ecliptic; (2) magnetic-sectored in 16 azimuthal bins, projected in the ecliptic; and (3) Sun-sectored in 32 bins, 8 in azimuth by 4 in elevation.

Since we determine on board the particle species, energy interval, and arrival direction, it is possible to accumulate angular distributions for any of the 150 identified species and energy bins. In practice, however, we are limited by telemetry space and only sector major species such as H, He, O, and Fe. In this paper, we report only magnetically sectored data for these four species; two energy intervals for He are included.

In order to avoid any aliasing in the onboard sectoring, all LEMT data read out in a telemetry frame are accumulated during an integral number of spins, the number of spins varying from frame to frame as required. Sectored data are accumulated on board in 32 bit registers that are compressed for telemetry using a block-normalization scheme. The largest sector count is located and shifted to fill a single 8 bit byte. All remaining sectors are then shifted by the same number of bits, and these sector bytes, plus the shift count, are telemetered. Thus, 16 sectored data are transmitted as a 17 byte quantity for each (46 or 92 s) major frame. This scheme provides a worst case error of $\sim 1\%$ near isotropy and the ratio of maximum-to-minimum sectored rates cannot exceed 128 in the worst case.

REFERENCES

Berdichevsky, D., et al. 1999, J. Geophys. Res., 104, 463
Burlaga, L. F., Ogilvie, K. W., & Fairfield, D. H. 1969, ApJ, 155, L171
Fisk, L. A. 1979, in Solar System Plasma Physics, Vol. 1, ed. E. N. Parker, C. F. Kennel, & L. J. Lanzerotti (Amsterdam: North Holland), 177
Fisk, L. A., & Jokipii, J. R. 1999, Space Sci. Rev., 89, 125
Giacalone, J., & Jokipii, J. R. 1999, ApJ, 520, 204
Giacalone, J., Jokipii, J. R., & Mazur, J. E. 2000, ApJ, 532, L75
Gloeckler, G., et al. 1999, Geophys. Res. Lett., 26, 157
Gordon, B. E., Lee, M. A., Möbius, E., & Trattner, K. N. 1999, J. Geophys. Res., 104, 28263
Gosling, J. T. 1993, J. Geophys. Res., 98, 18949
Jokipii, J. R., & Parker, E. N. 1969, Phys. Rev. Lett., 21, 44
Kahler, S. W. 1992, ARA&A, 30, 113
———. 1994, ApJ, 428, 837
Kahler, S. W., Sheeley, N. R., Jr., Howard, R. A., Koomen, M. J., Michels, D. J., McGuire, R. E., von Rosenvinge, T. T., & Reames, D. V. 1984, J. Geophys. Res., 89, 9683
Kennel, C. F., Coroniti, F. V., Scarf, F. L., Livesey, W. A., Russel, C. T., Smith, E. J., Wenzel, K.-P., & Scholer, M. 1986, J. Geophys. Res., 91, 11917
Leamon, R. J., Smith, C. W., Ness, N. F., Matthaeus, W. H., & Wong, H. K. 1998, J. Geophys. Res., 103, 4775
Lee, M. A. 1983, J. Geophys. Res., 88, 6109
———. 1997, in Coronal Mass Ejections, ed. N. Crooker, J. A. Jocelyn, & J. Feynman (Geophys. Monograph 99; Washington, DC: AGU), 227
———. 2000, in AIP Conf. Proc. 528, Acceleration and Transport of Energetic Particles Observed in the Heliosphere, ed. R. A. Mewaldt, J. R. Jokipii, M. A. Lee, E. Moebius, & T. H. Zurbuchen (New York: AIP), 3
Mason, G. M., Ng, C. K., Klecker, B., & Green, G. 1989, ApJ, 339, 529
Melrose, D. B. 1980, Plasma Astrophysics, Vol. 1 (New York: Gordon & Breach)
Ng, C. K., & Reames, D. V. 1994, ApJ, 424, 1032
Ng, C. K., Reames, D. V., & Tylka, A. J. 1999a, Geophys. Res. Lett., 26, 2145
———. 1999b, Proc. 26th Int. Cosmic Ray Conf. (Salt Lake City), 6, 151
Reames, D. V. 1990, ApJ, 358, L63
———. 1995, Rev. Geophys. Space Phys., 33, 585
———. 1997, in Coronal Mass Ejections, ed. N. Crooker, J. A. Jocelyn, & J. Feynman (Geophys. Monograph 99; Washington, DC: AGU), 217
———. 1999, Space Sci. Rev., 90, 413
———. 2000, ApJ, 540, L111
Reames, D. V., Barbier, L. M., & Ng, C. K. 1996, ApJ, 466, 473
Reames, D. V., & Ng, C. K. 1998, ApJ, 504, 1002
Reames, D. V., Ng, C. K., & Tylka, A. J. 2000, ApJ, 531, L83
Stix, T. H. 1962, The Theory of Plasma Waves (New York: McGraw-Hill)
Tan, L. C., & Mason, G. M. 1993, ApJ, 409, L29
Tan, L. C., Mason, G. M., Gloeckler, G., & Ipavich, F. M. 1989, J. Geophys. Res., 94, 6554
Tylka, A. J., Boberg, P. R., Adams, J. H., Jr., Beahm, L. P., Dietrich, W. F., & Kleis, T. 1995, ApJ, 444, L109
Tylka, A. J., Reames, D. V., & Ng, C. K. 1999a, Geophys. Res. Lett., 26, 2141
———. 1999b, Proc. 26th Int. Cosmic Ray Conf. (Salt Lake City), 6, 135
von Rosenvinge, T. T., et al. 1995, Space Sci. Rev., 71, 155